DR Methods

Whole rock trace elemental analyses: Whole rock analyses were conducted utilizing Laser Ablation ICP-MS coupled to a Merchanek 213nm UV laser and ICP-OES using a JY Horiba Ultima-2 instrument at the element analysis facility, University of Cardiff.

PIXE elemental analyses: *In situ* elemental mapping was undertaken on 60-80 µm-thick rock sections liberated from their glass slides utilizing Proton Induced X-ray Emission (PIXE) spectrometry, under operating conditions of 3 MeV energy, beam diameter 1 µm and variable scan area (50-300 μm^2), at the Applications Interdisciplinaires des Faiseaux d'Ions en Région Aquitaine (AIFIRA) facility, Centre des Etudes Nucléaires à Bordeaux-Gradignan, France.

***In situ* C and S isotopes:** *In situ* $\delta^{13}C$ and $\delta^{34}S$ measurements were made on polished thin sections and a solid rock surface using a Cameca 1280 HR microprobe at the CRPG, Nancy. Operating conditions were as follows: primary beam Cs+ 10nA, 10kV, focused on 10mm, with a 10mm raster; field aperture 2500 (image field 25 mm); secondary negative ions with a mass resolution of 4500, energy slit 50 eV, measured on FC2 (10^11) and with EM ion counting; EGUN 10kV, sample current <2 mA.

FIGURES

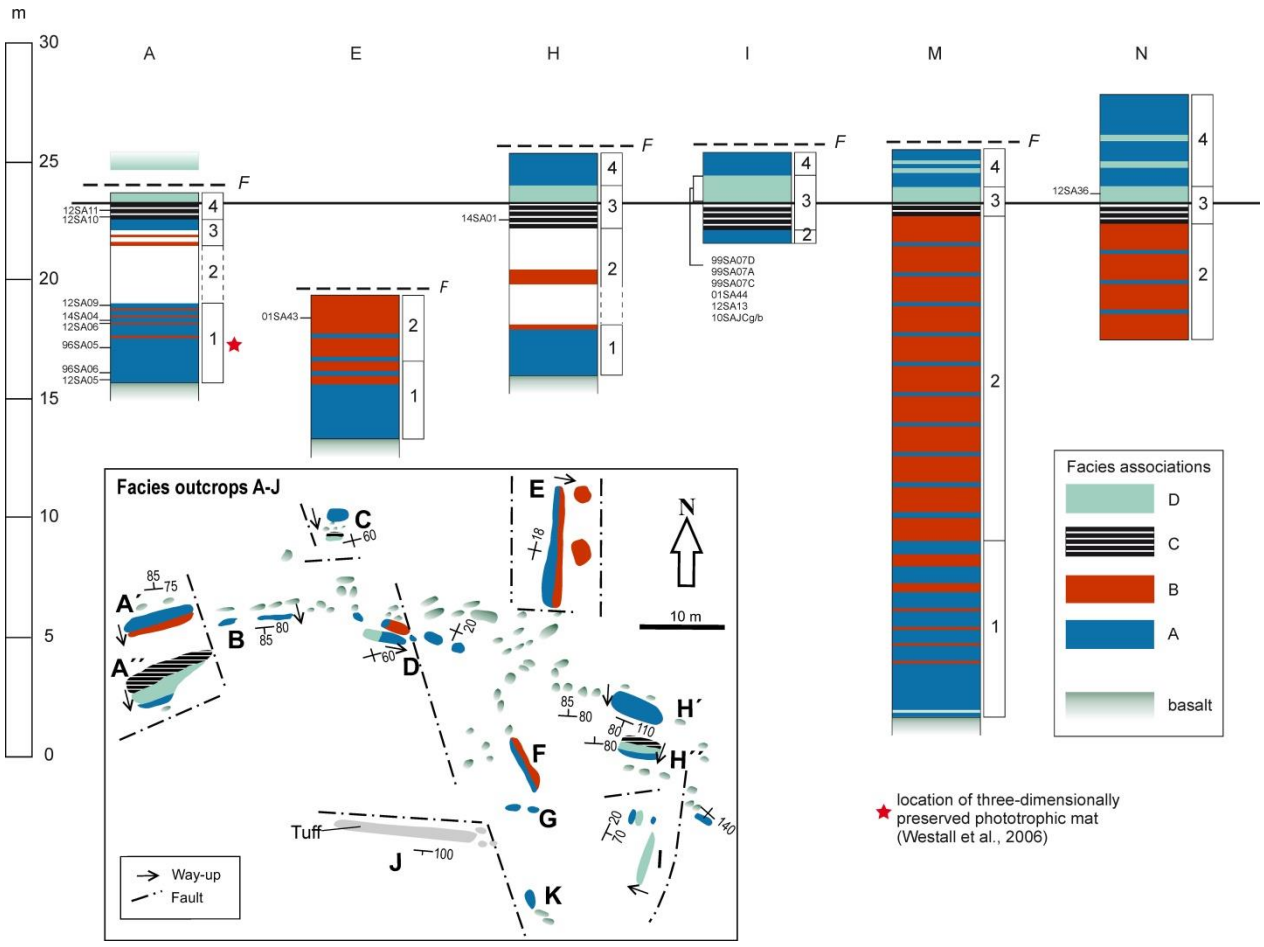

Figure DR 1. Correlation of selected stratigraphic columns in the study area and inset map of outcrops A-K.

Correlation based on specific, laterally continuous horizons of tuffaceous sediments in Facies D (black correlation line); sample locations are noted (Table DR2) to left of columns while sedimentary units (1-4) are indicated to right of columns; star indicates position of the phototrophic fossil mat described in Westall et al. (2006, 2011a); *F* delineates fault truncation of strata. Inset: detailed outcrop map (A-J, Fig. 1) confirming stratigraphic consistency despite

fault dissection; location of outcrop N, 1.5 km NE of inset area shown here, is indicated in Fig. 1C.

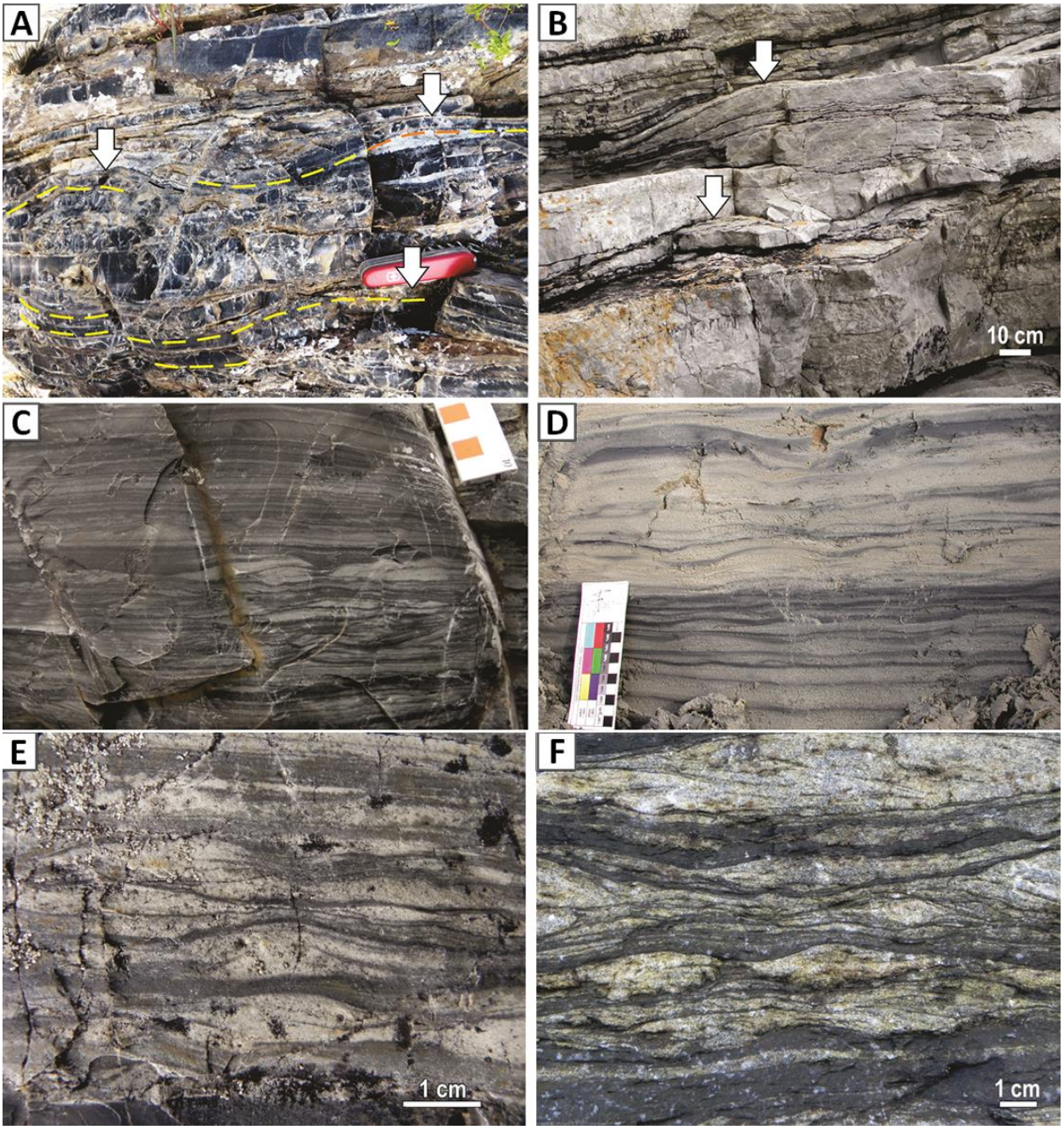

Figure DR 2. Comparison of Josefsdal Chert (JC) sedimentary textures with paleoenvironmentally diagnostic physical sedimentary structures in younger, analogous strata.

A, HCS-SCS sedimentary structures in JC Facies A. **B**, HCS-SCS in the Ordovician Grès Armoricain Formation, France. **C**, Parallel laminated and ripple cross-stratification of JC Facies

D. **D**, Modern tidal rhythmites and storm sands, Mont-Saint-Michel Bay, France. **E**, Oscillatory ripples and cross-laminae in JC Facies D. **F**, Oscillatory ripples and cross-laminae in the Ordovician Grès Armoricain Formation.

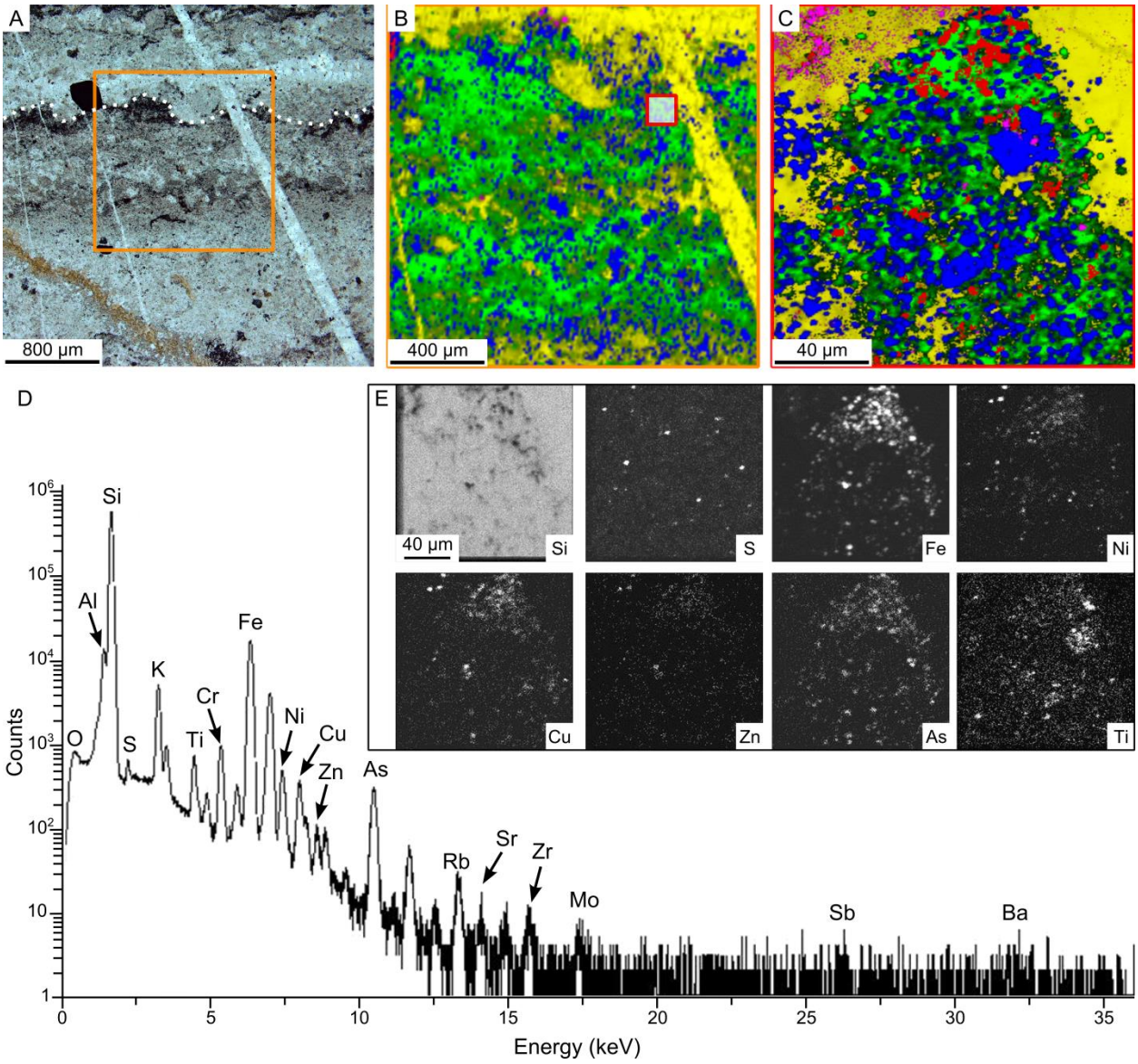

Figure DR3. Raman and PIXE analyses of Facies D strata containing the carbonaceous remains of a poorly preserved phototrophic biofilm. **A.** Optical micrograph showing visible concentration of carbonaceous matter and microcrystalline pyrite crystals in a phototrophic biofilm (dotted white line). Orange box denotes area of Raman map in **B**. **B.** Raman map of the phototrophic biofilm area documenting the presence of carbon (kerogen) in green, anatase in blue, quartz in yellow and pyrite in red. The red-outlined box denotes the area of a detailed Raman scan in **C** and the PIXE elemental maps in **E**. **C**. Portion of the carbonaceous biofilm

showing heterogeneous distribution of pyrite and anatase, the latter derived from alteration of volcanic protoliths. Note that the composition of the cross-cutting quartz vein is different from that of the cementing quartz matrix, which also contains muscovite, representing diagenetically and metamorphically altered volcanic clay-silt sized particulate matter. **D.** PIXE spectrum of the area shown in **C** documenting the presence of hydrothermal signatures, such as As and Ni (as well as Cu and Zn in this example). Note that this spectrum is typical of many samples across all Josefsdal sedimentary facies. **E.** PIXE maps (acquired for 12 h) of selected elements to show the pervasive silicification (Si), the heterogeneous distribution of pyrite (Fe and S) and anatase (Ti), as well as the concentration of hydrothermal tracer elements, e.g. Ni, As, Cu and Zn. Note that these elements do not occur in the later quartz vein that cuts diagonally across the biofilm layer and can be seen in the upper right hand corner of the PIXE maps. This late vein is also hydrothermal in origin but the siliceous fluids that filled it must have had a different source than the hydrothermally influenced, siliceous pore waters that cemented and lithified the Josefsdal sediments.

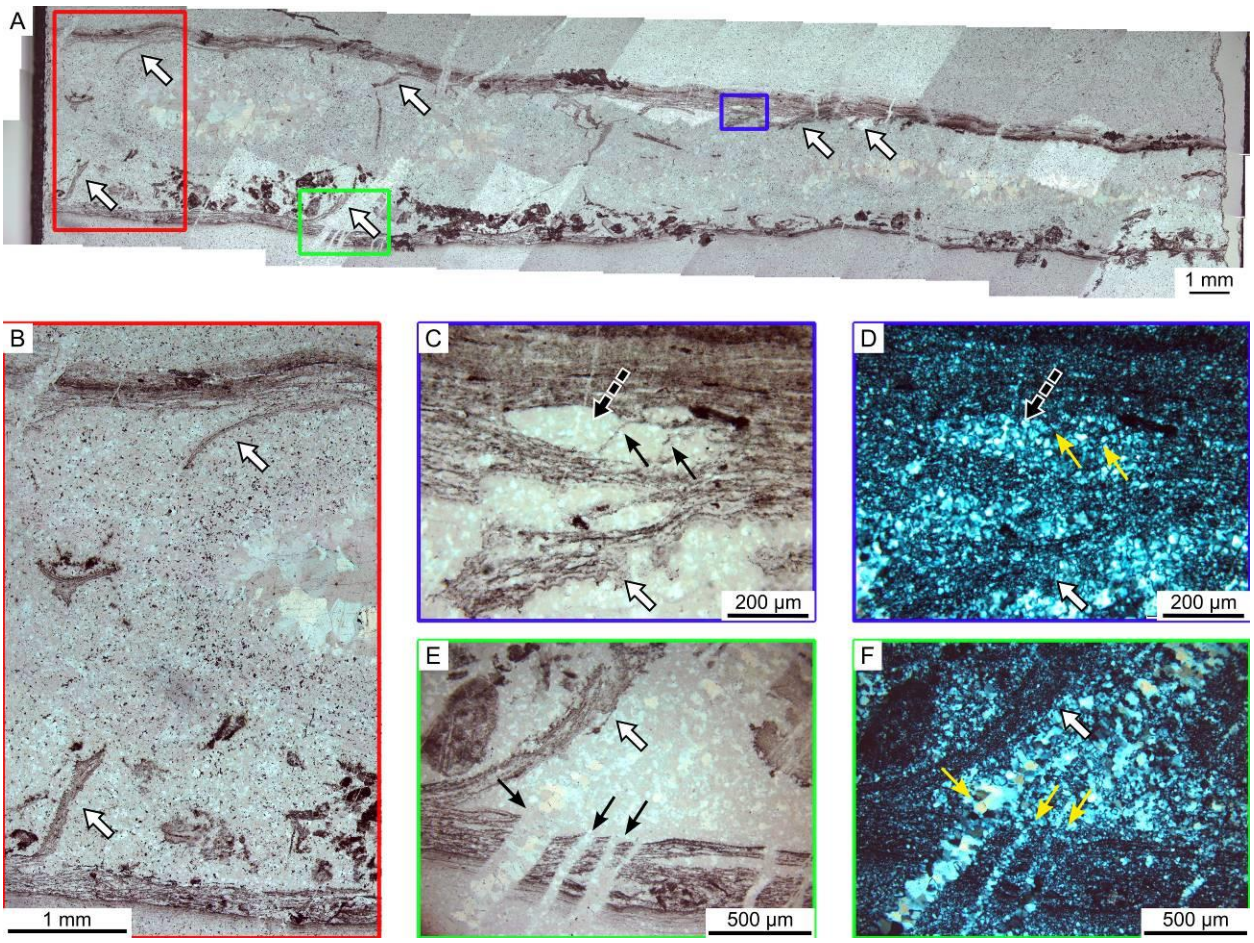

Figure DR4. Deformation of a pliable, living phototrophic biofilm. **A.** Optical micrograph view of a finely laminated photosynthetic biofilm that has been forcefully torn apart while it was still soft and probably living (Facies A, exposure L); white arrows indicate visibly torn fragments. The boxes denote details shown in B-F. **B.** The orientations of these biofilm fragments, one facing down and the other stretched upwards, illustrates the dynamic nature of the deformation. **C, D.** Transmitted and crossed polarized light microscopy of a portion of the biofilm showing a torn fragment (white arrow) and fluid infiltration causing opening of an oval, fluid-filled space (vug) in the biofilm (dashed black arrow). The small black arrows point to thin portions of the organic film stretched between the walls of the vug. **E, F.** Transmitted and crossed polarized

light microscopy of a portion of the biofilm showing a torn fragment (white arrow) and later, , cross-cutting quartz veins (small black arrows).

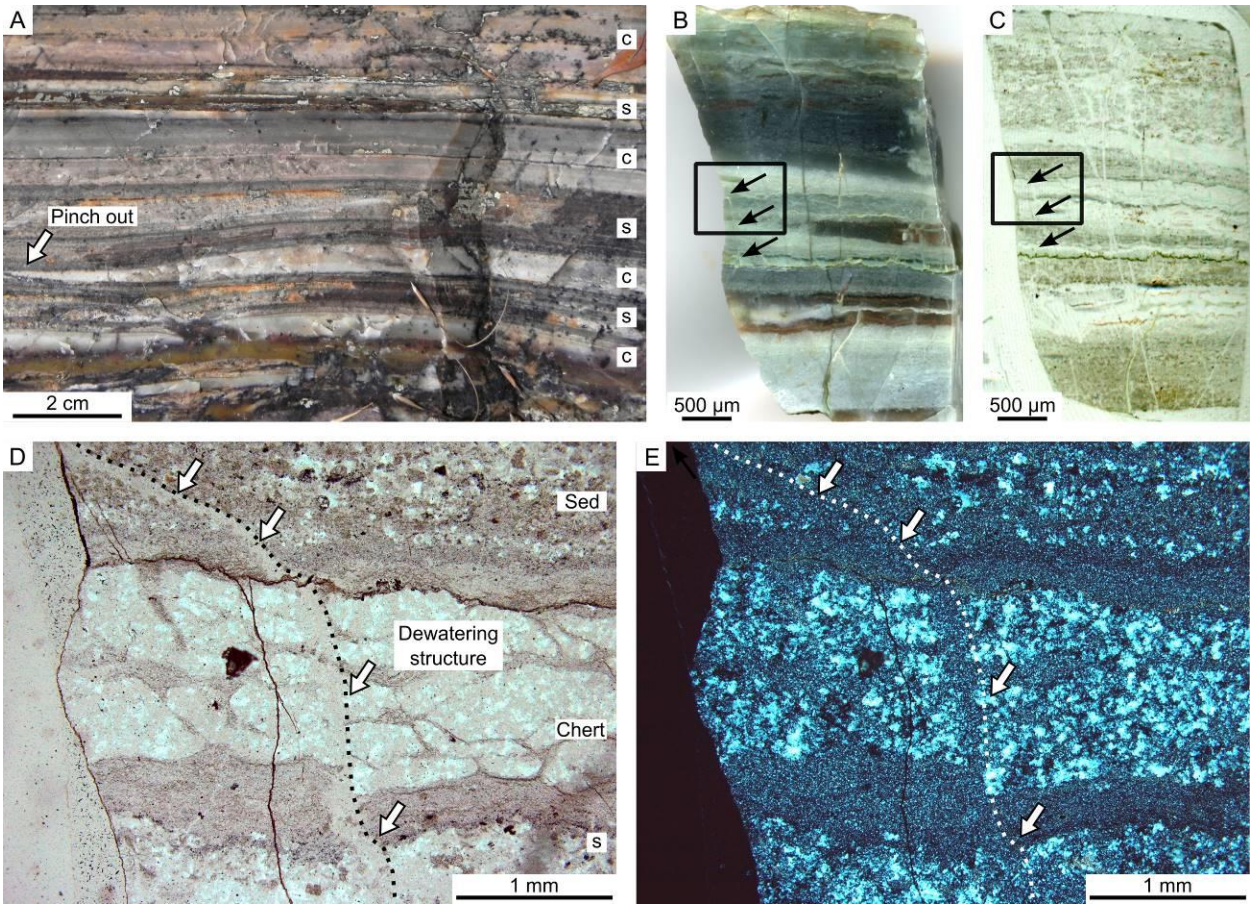

Figure DR5. Contemporaneous and early diagenetic silica deposition and infiltration, Facies B. **A**. Field view showing parallel infiltration of hydrothermal fluids into laminated sediments of Facies B. The pinchout of the chert layer © indicates that the parellel laminated sediments (S) must have been partially lithified at the time of infiltration. **B**. Hand specimen and optical micrograph view (**C)** of a sample from Facies B showing the alternation between sediment and chert layers and the location of a dewatering structure (box and arrows) shown in detail in **D** and **E. D, E.** Transmitted and polarize light microscopy detail of the thin section in (**C**) showing a dewatering feature (arrows and dotted black line) crossing both chert and sediment layers, indicating that they were contemporaneous.

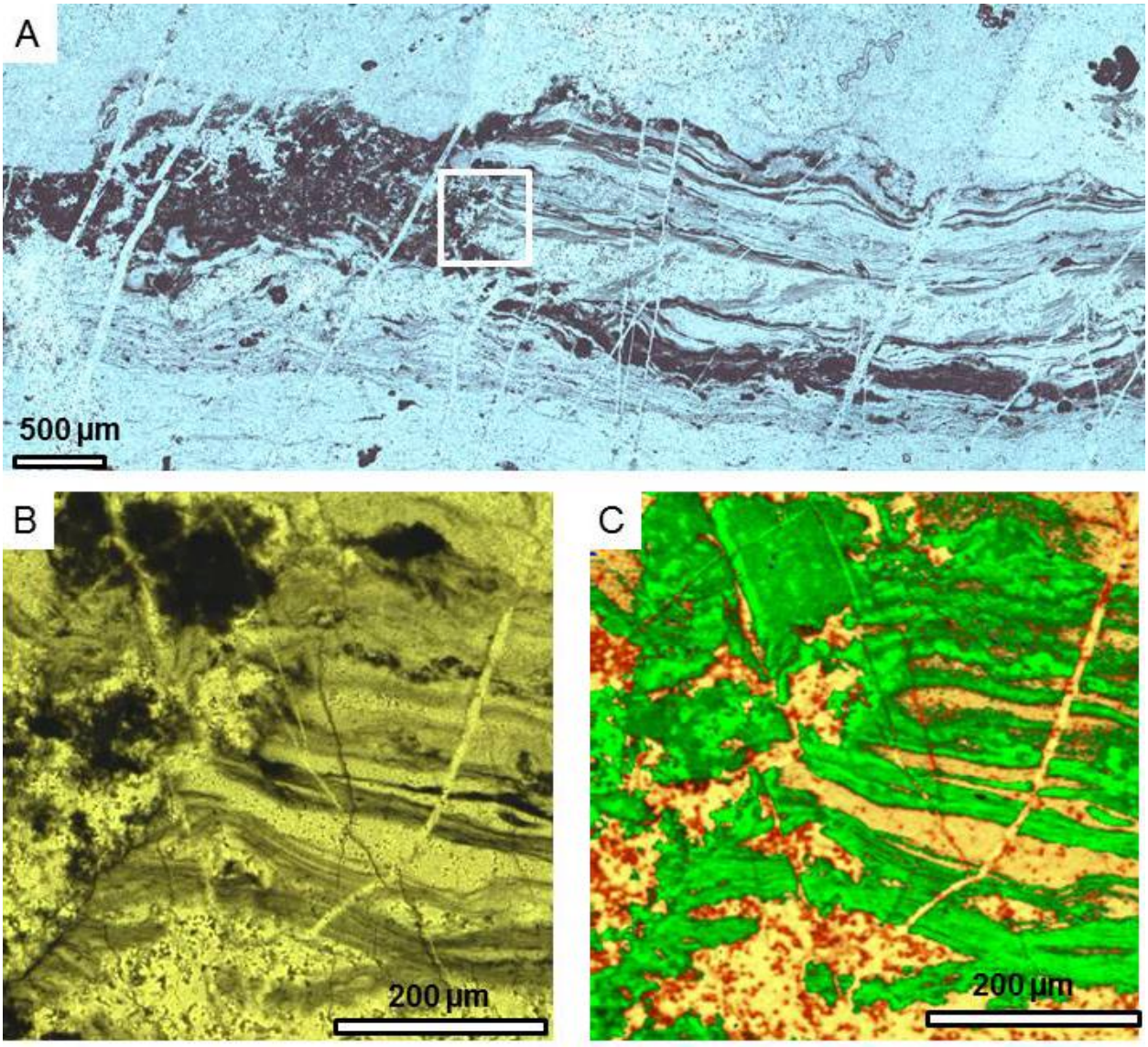

Figure DR 6. Details of a carbonacous biofilm, in a hydrothermally influenced horizon of Facies A.

A. Optical micrograph displaying a portion of a photosynthetic biofilm juxtaposed with a clotted layer of chemotrophic colonies, formed in an inferred hydrothermal silica gel (white arrow in DRFig. 7A). **B, C.** Optical micrograph and Raman map (carbon – green, quartz – yellow) of the area outlined by white box in **A** showing the torn edge of the phototrophic biofilms and some spatially affiliated chemotrophic clots.

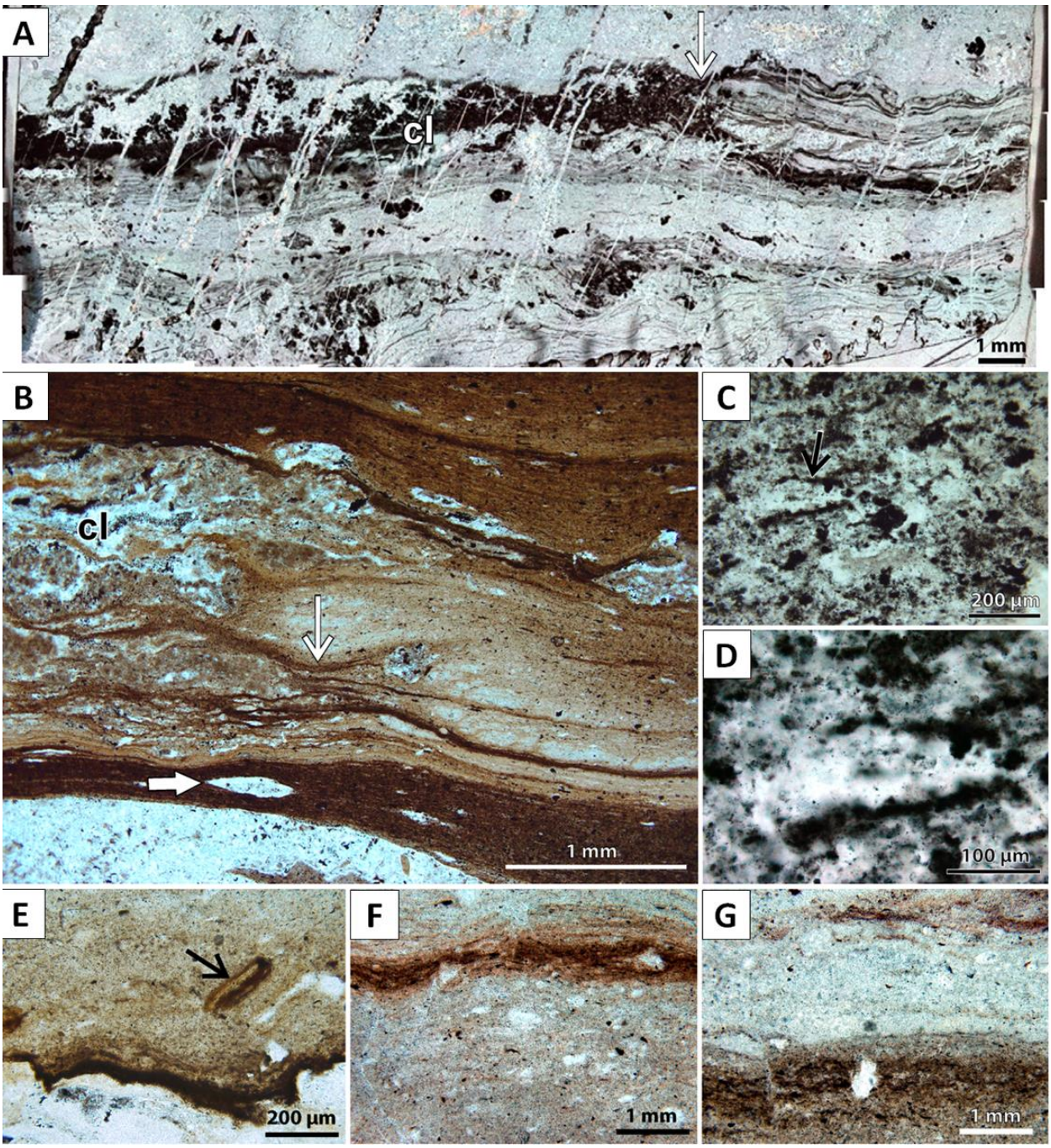

Figure DR7. Microbial microtextures of Josefsdal Chert and Late Jurassic siliceous sinter fabrics, Argentina.

A,. Juxtaposed JC *Type 1* laminated mat and *Type 2* clots (cl) in an inferred silica gel horizon of hydrothermal origin in Facies A (arrow shows location of detail in DRFig. 3A, B).

B. San Agustín sinter, Argentina: dark brown (carbonaceous), phototrophic, wavy laminated mats (chert-filled, fossil O_2-gas bubble indicated by thick arrow) with juxtaposed light brown (carbonaceous), clotted (cl) microbial fabric (arrow), reminiscent of similar structure in **A**.

C, D. Clotted carbonaceous *Type 2* fabric in JC hydrothermal Facies C consisting of volcanic clasts (arrow in **C),** interpreted as chemolithtrophic colonies. **E.** Eroded laminated phototrophic mat fragment (arrow), La Marciana sinter, Argentina, similar to JC feature in Fig. 3F. **F,G.** White detrital mineral grains incorporated into dark, wavy phototrophic laminated mats, La Marciana sinter, Argentina, similar to those occurring in JC *Type 1* phototrophic mats (Fig. 3B).

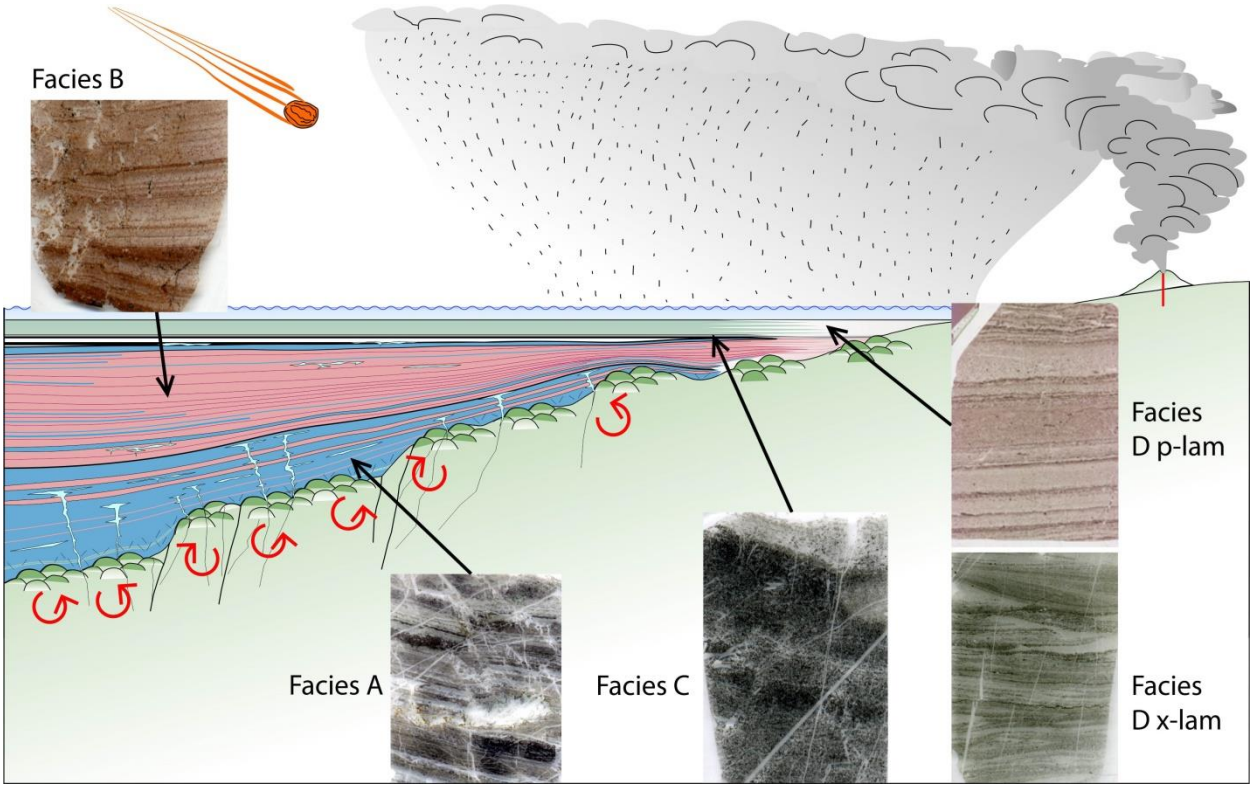

Figure DR8. Sketch showing volcanogenic sediments in an inferred, hydrothermallyinfluenced, nearshore depositional environment, 3.33Ga Josefsdal Chert, South Africa.

Representative, standard-sized (entire) thin section photographs illustrate sedimentary (chert) facies associations, A-D (Fig. 2) (p-lam, parallel-laminae; x-lam, ripple cross-laminae). Red arrows indicate hydrothermal circulation of Si-enriched seawater through uppermost basalt pillow lavas as primary source of silicification. Possible influence of impact-related hydrothermal activity shown (Sleep and Lowe, 2014; Lowe et al., 2014).

Table DR1. **Description of Josefsdal Chert sedimentary facies associations and their hydrothermal and microbial fossil associations.**

Facies associations	A	B	C	D
Grain size	Well-sorted, fine to medium sand	Poorly sorted, silt/clay to medium sand	Fine to medium sand	Normally graded, silt to fine to coarse sand
Mineralogy	>99% quartz with trace pyrite, anatase and barite; pseudomorphed volcanic clasts; chert matrix	>99% quartz with trace pyrite, anatase and barite; pseudomorphed volcanic clasts; chert matrix	>98% quartz with trace anatase; pseudomorphed volcanic clasts in silicified clay/silt matrix	>96% quartz with minor pyrite, and trace anatase and rutile; gray layers: silica-replaced volcanic clasts; black layers: carbonaceous chert
Elemental composition	>99% Si; trace Al, Fe, K, Mg, Ca	>99% Si; trace Al, Fe, K	>95% Si; minor Al; trace Fe, K, Ti, Mg, Ca	>96% Si; minor Al; trace Fe, K, Ti, Mg, Ca, Na
Lithofacies characterization	Swaley to hummocky cross-stratification (dm amplitude, several dm to m wavelength)	Regular, parallel laminated to thinly bedded (cm to dm thickness), in thickening-thinning bundles; gutter casts in some sections	Black and white banded chert; precursor sediment laminated with current ripples	Normally graded beds (mm to cm thick) composed of small lapilli alternating with oscillatory ripples to flaser beds (mm to cm thickness)
Thickness	1m to up to several m, depending on outcrop	several dm, up to several m (mainly interbedded with SCS-HCS of A)	10s of cm	metric
Colour	Blue/black	Reddish (Fe-stained)	Black and white	Alternating greenish grey and black laminae
Inferred environment of deposition	Tempestites formed in upper offshore to shoreface zone	Fairweather shoreface with tidal influence	Upper shoreface; moderate energy	Gray, graded, parallel laminated: settling of volcanic ash fall and lapilli; dark ripples: current and wave reworking of volcaniclastics under current (tidal) action; upper shoreface to foreshore
Hydrothermal features	Pervasive silicification (>99% SiO_2) + presence of Fe, K, Ni, positive La, Eu, Gd, Y, depleted LREEs; thin, white, stockwork-like veins in subjacent basalt and lower Unit 1; white to translucent vertical chert dykes and bedding-parallel sills in Facies A tracing swaley seafloor palaeotopography	Pervasive silicification (>99% SiO_2) + presence of Fe, K, Ni, positive la, Eu, Gd, Y, depleted LREEs; some bedding-parallel white chert sills	Laterally variable silicification) + presence of Fe, K, Ni, positive la, Eu, Gd, Y, depleted LREEs; localized, lateral infiltrations of chert veins to produce cm-scale black and white banding	Silicification + presence of Fe, K; Ni, positive La, Eu, Gd, Y, depleted LREEs; with some minor cross-cutting and bedding parallel, white chert infiltration
Microbial types	*Type 1* laminated, inferred photosynthetic biofilms (associated organotrophs, Westall et al., 2011a); rare *Type 2*, inferred chemotrophic clots; *Type 3* detrital carbonaceous fragments	*Type 1* laminated, inferred photosynthetic biofilms at the tops of sandier layers; *Type 2* clots in poorly sorted, fine-grained horizons; *Type 3* detrital carbonaceous fragments (clots, biofilms)	Mixed, inferred chemotrophic/ phototrophic biofilms; locally high biomass	*Type 1* laminated, inferred photosynthetic biofilms at the tops of sandier layers; *Type 3* detrital carbonaceous fragments (clots, biofilms)
Stratigraphic relationships	Main sedimentary facies of Unit 1, deposited on top of silicified basalt at base of sedimentary succession; prevalent in	Infilling the swales of Facies A; predominant deposit of Unit 2	Caps Unit 2	Predominant deposit of Unit 3; thinly interbedded with Facies A and C in Unit 4

	Unit 4			

Table DR2. Major and trace element composition of Josefsdal Chert samples compared with an underlying silicified basalt sample.

A, B. Major oxides (wt%) and trace element (ppm) data. Note that As was not analyzed.

C. Shale-normalised (mud of Queensland, MUQ; Bohlar et al., 2005) rare earth element and yttrium (REE + Y) patterns (ppm) show positive Y and Eu anomalies.

A. Major oxides (wt %)

	Sample #	SiO_2 wt%	TiO_2 wt%	Al_2O_3 wt%	Fe_2O_3 wt%	MnO wt%	MgO wt%	CaO wt%	Na_2O wt%	K_2O wt%	P_2O_5 wt%	LOI wt%	Total wt%
Underlying basalt													
	12SA01	92.66	0.88	2.94	2.11	0.06	0.52	0.05	0.05	0.51	0.032	1.00	100.82
Facies A													
	12SA06	98.95	0.01	0.26	0.07	0.02	0.09	0.13	0.06	0.06	0.002	0.39	100.03
	12SA06B Hydro	97.49	0.01	0.09	0.75	0.05	0.11	0.15	0.03	0.03	0.002	0.43	99.15
	12SA16	99.29	0.01	0.15	0.22	0.02	0.05	0.05	0.01	0.05	0.009	0.23	100.09
	12SA20	99.94	0.01	0.07	0.71	0.01	0.02	0.05	0.03	0.03	0.005	0.39	101.27
	12SA32	85.51	0.04	0.53	10.61	0.13	0.03	0.11	0.04	0.14	0.033	2.15	99.31
	12SA34	95.71	0.03	0.59	1.77	0.02	0.05	0.04	0.03	0.15	0.013	0.83	99.24
Facies B													
	12SA22	87.64	0.02	0.58	10.50	0.02	0.08	0.06	0.03	0.08	0.015	1.91	100.95
Facies C													
	14SA01	96.77	0.05	1.35	0.08	0.01	0.05	0.08	0.19	0.31	0.009	0.44	99.34
Facies D													
	10SAJC g/b	96.47	0.17	1.67	0.12	0.01	0.08	0.09	0.04	0.50	0.003	0.38	99.53
	12SA13	96.35	0.20	1.74	0.72	0.01	0.10	0.17	0.06	0.53	0.003	0.61	100.50
	12SA24g	91.63	0.29	2.80	0.18	0.01	0.07	0.05	0.07	0.77	0.010	0.70	96.58
	12SA24b	98.03	0.15	1.72	0.21	0.01	0.03	0.03	0.06	0.47	0.002	0.55	101.26
	12SA36	98.36	0.19	1.46	0.10	0.01	0.06	0.04	0.05	0.38	0.008	0.52	101.18

Standards	SiO_2	TiO_2	Al_2O_3	Fe_2O_3	MnO	MgO	CaO	Na_2O	K_2O	P_2O_5	LOI	Total
JB1a	52.35	1.30	14.47	9.34	0.16	7.84	9.48	2.77	1.40	0.241	0.78	100.13
JG1a	72.57	0.24	14.17	2.00	0.06	0.66	2.14	3.29	3.93	0.074	0.50	99.65

Certified/Preferred values	SiO_2	TiO_2	Al_2O_3	Fe_2O_3	MnO	MgO	CaO	Na_2O	K_2O	P_2O_5	LOI	Total
JB1a	52.16	1.30	14.51	9.10	0.15	7.75	9.23	2.74	1.42	0.25	0.78	99.39

B. Trace elements

	Sample #	Sc ppm	V ppm	Cr ppm	Co ppm	Ni ppm	Cu ppm	Zn ppm	Sr ppm	Y ppm	Zr ppm	Ba ppm
Underlying basalt												
	12SA01	5.9	99.4	456.9	16.6	86.6	151.0	41.2	7.2	10.0	52.5	27.8
Facies A												
	12SA06	0.8	4.3	38.3	1.8	257.3	4.9	7.5	2.2	0.9	9.2	5.7
	12SA06B Hydro	0.5	1.9	71.7	3.4	37.6	16.5	12.4	2.1	0.7	10.8	5.6
	12SA16	0.4	4.4	20.6	1.1	14.7	44.2	31.5	0.4	0.4	5.6	3.2
	12SA20	0.3	3.2	26.9	1.2	25.7	16.8	33.7	1.3	0.4	3.8	7.6
	12SA32	2.4	10.2	46.7	7.1	70.8	20.2	29.2	17.5	3.7	10.9	47.5
	12SA34	0.8	12.1	64.0	11.0	56.9	22.9	11.0	1.2	1.0	8.9	19.3
Facies B												
	12SA22	2.3	16.7	26.5	4.2	40.3	60.6	28.6	2.0	5.1	9.8	3.6
Facies C												
	14SA01	1.6	11.9	17.7	1.6	14.7	8.3	12.5	2.5	0.6	6.1	10.7
Facies D												
	10SAJC g/b	3.0	35.3	329.9	30.8	130.4	32.5	24.1	4.7	1.7	14.8	115.8
	12SA13	4.6	59.0	293.0	43.4	107.9	41.7	32.1	3.8	2.1	23.2	33.1
	12SA24g	6.0	77.2	499.1	16.0	46.4	19.5	19.3	2.4	3.6	26.0	37.0
	12SA24b	3.1	40.0	304.8	44.3	125.3	30.4	88.2	1.9	1.8	19.4	29.8
	12SA36	4.3	38.6	409.1	60.6	120.4	32.5	26.6	1.9	1.7	18.9	26.4

Standards	**Sc**	**V**	**Cr**	**Co**	**Ni**	**Cu**	**Zn**	**Sr**	**Y**	**Zr**	**Ba**
JB1a	28.1	203.0	421.1	39.7	142.8	57.5	77.7	449.2	24.4	142.1	507.9
JG1a	5.9	21.5	13.4	6.3	5.0	1.8	38.6	179.5	32.0	123.3	465.1

Certified/Preferred values	**Sc**	**V**	**Cr**	**Co**	**Ni**	**Cu**	**Zn**	**Sr**	**Y**	**Zr**	**Ba**
JB1a	27.9	206.0	415.0	39.5	134.0	55.0	82.0	443.0	24.0	146.0	497.0

C. REE + Y values (ppm)

	Hydrothermal chert		Facies A					
			Outcrop A		Outcrop L		Outcrop N	
	12SA29	12SA06B Hydro	12SA06	12SA16	12SA20	12SA32	12SA34	12SA37
La	0.003	0.027	0.029	0.014	0.003	0.063	0.017	0.042
Ce	0.002	0.014	0.020	0.008	0.002	0.050	0.013	0.029
Pr	0.002	0.019	0.025	0.011	0.002	0.051	0.015	0.039
Nd	0.003	0.015	0.019	0.007	0.003	0.051	0.016	0.040
Sm	0.004	0.010	0.015	0.007	0.006	0.060	0.022	0.044
Eu	0.006	0.013	0.019	0.013	0.006	0.108	0.045	0.076
Gd	0.006	0.009	0.013	0.008	0.006	0.075	0.024	0.050
Tb	0.010	0.010	0.010	0.010	0.010	0.081	0.020	0.061
Dy	0.007	0.010	0.014	0.007	0.008	0.090	0.029	0.061
Y	0.009	0.022	0.030	0.013	0.012	0.117	0.030	0.081
Ho	0.008	0.008	0.016	0.008	0.008	0.090	0.025	0.057
Er	0.006	0.015	0.015	0.012	0.009	0.086	0.021	0.062
Tm	*bd*	0.020	0.020	0.020	*bd*	0.098	0.020	0.059
Yb	0.009	0.018	0.018	0.012	0.012	0.089	0.022	0.062
Lu	*bd*	0.020	0.020	0.020	0.020	0.082	0.020	0.061

	Facies B	Facies C	Facies D					Underlying basalt
	Outcrop K	Outcrop H	Outcrop I	Outcrop I	Outcrop L		Outcrop N	
	12SA22	14SA01	10SAJC g/b	12SA13	12SA24g	12SA24b	12SA36	12SA01
La	0.042	0.031	0.039	0.081	0.084	0.182	0.033	0.265
Ce	0.034	0.021	0.037	0.074	0.077	0.163	0.036	0.255
Pr	0.051	0.021	0.038	0.077	0.079	0.162	0.038	0.265
Nd	0.054	0.017	0.036	0.075	0.076	0.157	0.040	0.256
Sm	0.084	0.020	0.045	0.074	0.092	0.154	0.049	0.231
Eu	0.172	0.045	0.076	0.102	0.146	0.229	0.064	0.299
Gd	0.113	0.019	0.038	0.063	0.085	0.116	0.055	0.234
Tb	0.131	0.020	0.040	0.061	0.081	0.081	0.051	0.253
Dy	0.141	0.019	0.046	0.066	0.098	0.065	0.053	0.267
Y	0.159	0.020	0.053	0.064	0.112	0.055	0.052	0.314
Ho	0.139	0.016	0.041	0.057	0.082	0.049	0.041	0.238
Er	0.134	0.015	0.039	0.056	0.083	0.045	0.039	0.226
Tm	0.157	0.020	0.039	0.059	0.078	0.039	0.039	0.235
Yb	0.157	0.018	0.037	0.062	0.092	0.046	0.037	0.222
Lu	0.163	0.020	0.041	0.061	0.082	0.041	0.041	0.037

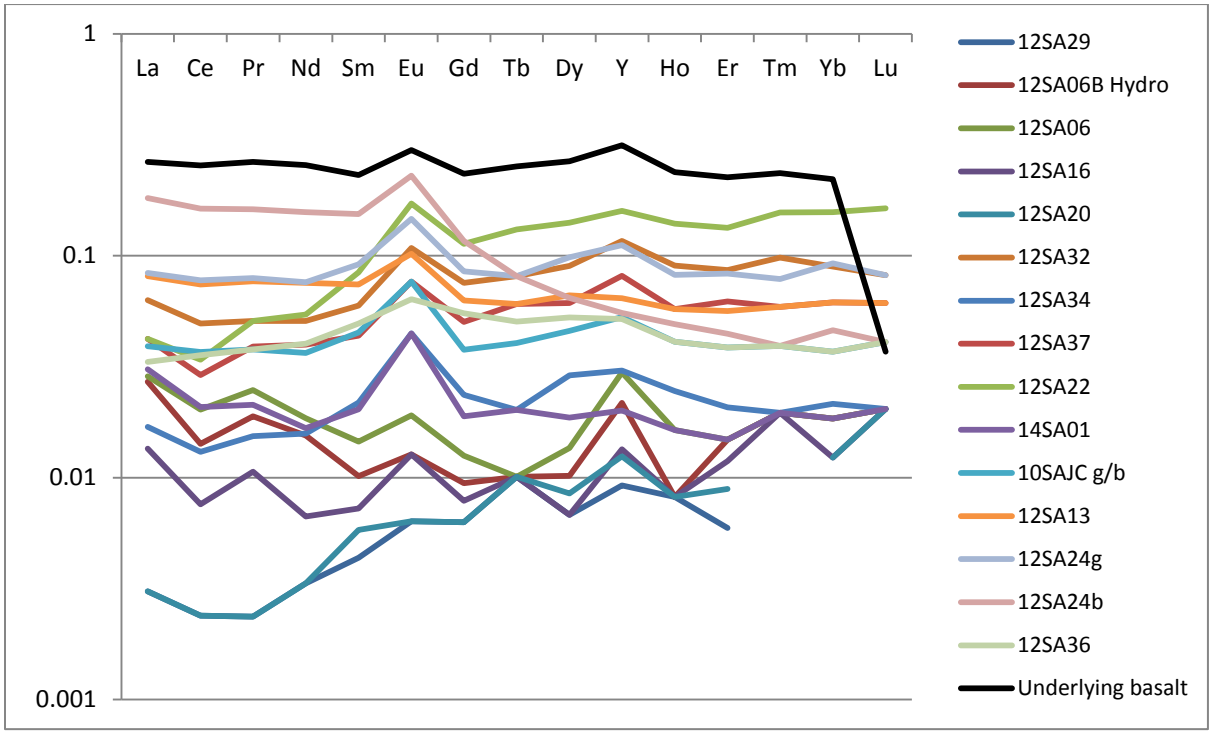

REE + Y elemental distributions for various samples. The MUQ-normalized (Bohlar et al., 2005), relatively flat distributions are typical for silicified volcanic protoliths (van den Boorn et al., 2007). All samples show slight to significant positive Eu and Y anomalies suggesting hydrothermal influence (cf. Hofmann and Bohlar, 2007).